# Speed of Sound Estimation at Multiple Angles from Common Midpoint Gathers of Non-Beamformed Data

Thurston Brevett*, Sergio J Sanabria*†, Rehman Ali*, Jeremy Dahl*
Email: tbrevett@stanford.edu, sanse@stanford.edu, Rehman_Ali@URMC.Rochester.edu, jjdahl@stanford.edu
* Department of Radiology, Stanford University, Stanford, CA, USA
† Deusto Institute of Technology, University of Deusto/Ikerbasque, Basque Foundation for Science, Bilbao, Spain

2022 IEEE International Ultrasonics Symposium (IUS) | 978-1-6654-6657-8/22/$31.00 ©2022 IEEE | DOI: 10.1109/IUS54386.2022.9958779

***Abstract*—Sound speed estimation is a promising quantitative parameter in ultrasound for both for it's potential as a biomarker, where sound speed is known to be correlated with biological changes, and for aberration correction, where knowledge of the sound speed allows for correction of distortions in the image. Previous methods for sound speed estimation rely on the use of an a-priori sound speed for beamforming, from which sound-speed estimates are then calculated. However, this assumption introduces a bias in the estimation technique, because errors in the a-priori sound speed lead to distortions in the image. Here we present a method for sound speed estimation that avoids this bias by estimating the sound speed without beamforming.**

***Index Terms*—sound speed estimation, beamforming, phase aberration**

## I. INTRODUCTION

Sound speed is a promising quantitative parameter in ultrasound that can be used as a biomarker or as a basis for phase aberration correction. Sound speed refers to the speed of propagation of compressional waves in tissue, which is a different quantity than the shear wave speed used in conventional ultrasound elastography. Sound speed has been shown to vary with biological changes, such as fat accumulation in the liver ( [1], [2]) and muscle ( [3]), and physio-pathological changes of tumors in the breast ( [4], [5]). Knowledge of the local sound speed can therefore be used to detect local changes in tissue. Conventional ultrasound systems assume a nominal sound speed value of 1540 m/s [6], while sound speed shows approximately $10\%$ variation in soft tissues. This divergence leads to aberrations in ultrasound images. Knowledge of the sound speed, locally or globally, can be used to correct for phase aberration effects in B-mode images.

There have been many recently proposed methods that seek to estimate the sound speed. The CUTE method [7] generates a series of plane-wave beamformed images at multiple angular directions, and then correlates the phase shifts across these images with changes in the speed of sound, and then finally inverts those changes to form a local sound speed estimate. Sanabria et. al [8] also correlate changes in the phase across full-synthetic aperture data beamformed with multiple transmit apertures with changes in the sound speed. Another method, IMPACT [9], generates beamformed images and estimates the global average sound speed as the sound speed that yields the maximum coherence for each pixel in the image, and then applies an inversion to compute the local sound speed from the global average for each pixel. A similar approach was proposed by Imbault et al [2] using retrospectively focused pulses to maximize the coherence factor.

However, creating images is highly sensitive to an accurate a-priori reference sound speed. This leads to spatial ambiguity, where a reflection at some position $\mathbf{p}$ is instead observed at a position $\mathbf{p}'$ in the beamformed image. For small deviations in the sound speed, this effect is small and can be safely ignored. For large deviations, however, this spatial ambiguity is non-neglible. Fig. 1 demonstrates this effect. For a sound speed variation of +/- 100 m/s, a point scatterer located at a depth 30mm shows a depth ambiguity of +/- 2mm. Furthermore, the shape of the point-spread function is also modified and the peak of the response no longer has zero-phase.

In this paper, we introduce a method of global sound speed estimation that avoids spatial ambiguity issues. Our method doesn't use beamforming or beamformed images with an a-priori sound speed, but instead correlates the full-synthetic aperture data directly to obtain an estimate of both the sound speed and the spatial location of the returned echos. Although we present this method applied to global sound speed estimation, the technique is applicable to local sound speed estimation.

## II. THEORY

### *A. Sound Speed Estimation from Time-of-flight Profiles - Triangulation for single scatterer case*

Without loss of generality, we discuss sound speed estimation with a one-dimensional ultrasound array of $N$ elements, each of which can be used both as a transmitter and a receiver. We consider the full synthetic aperture dataset consisting of a trace of samples in time captured for each combination of one transmit element and one receive element $V(t, i_{Tx}, j_{Rx})$. This represents the complete set of information that we are able to gather with the array, without introducing any dependence on our knowledge of the sound speed. To illustrate the sound

This research was funded with a NIH Grant R01-EB027100. Sergio J Sanabria was additionally funded by an Ikerbasque Fellowhsip, a grant DTS21/00076 (QUIOMICS) from the Spanish Ministry of Science and Innovation, and a Health Project 2021333036 (ECOFRAIL) from the Basque Government.

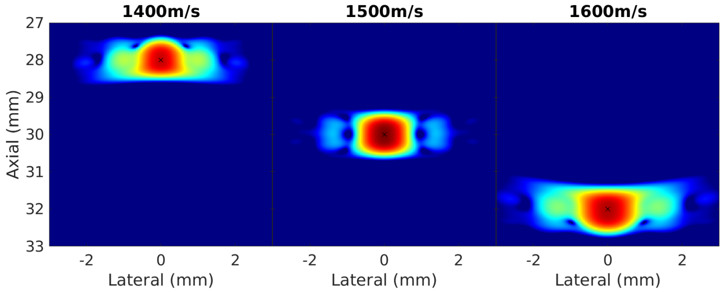


Fig. 1. Spatial ambiguity of scatterer point-spread function due to initial sound speed assumption: delay-and sum beamformed data for a point scatterer at a depth of 30 mm in a homogeneous medium with sound speed of 1500 m/s when the assumed sound speed in the beamforming step is (from top to bottom) 1400 m/s, 1500 m/s, and 1600 m/s with an apparent depth of 28 mm, 30 mm, and 32mm respectively.

speed estimation process, we first consider a medium with a constant sound speed $c_s$ and a single scatterer at a location $\mathbf{p_s}$. With the $N$ receive array elements located at $\mathbf{p_n} \in R^3, n \in N$, and the $M$ transmit elements co-located at $\mathbf{p_m} \in R^3, m \in M$, the time-of-flight for transmitter $m$ to receiver $n$ is given by (1). The total propagation time is simply the distance along a ray from $\mathbf{p_m}$ to $\mathbf{p_s}$ plus the distance along a ray from $\mathbf{p_s}$ to $\mathbf{p_n}$ scaled by the speed at which the wave propagates, $c_s$.

$$\tau_{mn}(c_s, \mathbf{p_s}) = c_s^{-1}\left(||\mathbf{p_s} - \mathbf{p_m}||_2 + ||\mathbf{p_n} - \mathbf{p_s}||_2\right) \quad (1)$$

Given these time-of-flight estimates between the transmit and receive apertures $\tau_{mn}$, we can estimate the sound speed and triangulate the scatterer location $(\hat{c_s}, \hat{\mathbf{p_s}})$ by finding the best fit scatterer location to (1) across all transmit-receive pairs.

As a particular case, suppose we have a linear array with all elements having a common midpoint at the origin $\mathbf{p} = \mathbf{0}$ and a scatterer that is axially aligned with the midpoint such that it is equidistant from the transmit and receive elements. We refer to this configuration as Common mid-point (CMP) gather. Then, we have

$$\mathbf{p_n} = -\mathbf{p_m} \quad (2)$$

$$||\mathbf{p_s} - \mathbf{p_m}||_2 = ||\mathbf{p_s} - \mathbf{p_n}||_2 \quad (3)$$

leading to a simplified expression given in (4).

$$\tau_n(c_s, \mathbf{p_s}) = 2c_s^{-1}||\mathbf{p_n} - \mathbf{p_s}||_2 \quad (4)$$

If we then square both sides of the expression and assume the receiver has no axial or elevation component (i.e. $y_n = z_n = 0$) and assume that the scatterer has no elevation or lateral component (i.e. $y_s = x_s = 0$), then (4) simplifies further to (5).

$$\tau_n^2(c_s, z_s) = 4\left(\frac{1}{c_s}\right)^2 x_n^2 + 4\left(\frac{z_s}{c_s}\right)^2 \quad (5)$$

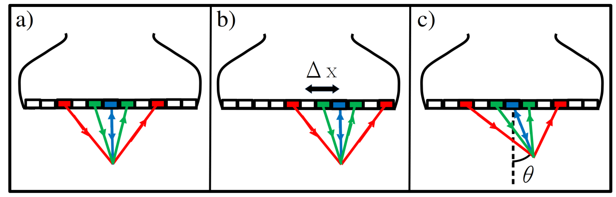


Fig. 2. Common mid-point (CMP) gather configurations. a) Axial CMP gathers with a midpoint at the center of the array. b) Axial CMP gathers with a midpoint offset by $\Delta x$ with respect to the center of the array. c) Non-axial CMP gathers originating at the common midpoint and steered at an angle $\theta$.

Equation (5) can be recognized as a parabolic function of $x_n$, where the coefficients of the parabola directly correspond to the sound speed $c_s$ and scatterer depth $z_s$. By fitting our time-of-flight estimates to (5) we obtain estimates of the corresponding global average sound speed and scatterer location. In the case of a scatterer tilted off-axis by an azimuth angle $\theta$ from the aperture center as in Fig. 2c, we instead solve (1) directly.

### *B. Sound Speed Estimation from Time-of-flight Profiles - Diffuse scattering media*

In real tissue imaging scenarios, the recorded ultrasound time traces are formed by aggregation of scattering signal at an asymptotically large number of scattering micro-structures, which is modeled as a diffuse scattering medium. In order to estimate the speed of sound by comparing ray paths along different directions, we first need to obtain a coherent signal for estimating phase shift.

It is known that across the receive aperture, volumetric diffuse scattering quickly becomes incoherent as we correlate receive channels laterally. The main purpose of the beamforming and image formation step in previous methods is to make the data coherent by combining the information across multiple transmits via summation. However, when the sound speed is not known a-priori, this can introduce large spatial ambiguity errors, as shown in Fig. 6.

Let us now consider the CMP gather traces introduced in the previous section. Rather than using the full set of data where we have a trace for each transmit and receiver pair, we consider only transmit elements and receive elements that share a common geometric midpoint. It is known in the literature that across the set of CMP gathers, ultrasound full-synthetic aperture data is highly coherent without summation. This is due to the fact that far-field echos from arbitrary reflectors arrive with a consistent phase distribution across different paths of the CMP gathers. Numerically, we estimate this time-of-flight profile via zero-normalized cross-correlation between pairs of elements across the aperture. Another advantage of the CMP gather aperture is that it introduces symmetry into the time-of-flight estimation problem for axial data. This symmetry allows one to use a parabolic fit to estimate the sound speed and spatial scattering location of the data.

### C. Spatio-Temporal Filtering for scatterer localization in diffuse media

Even if coherence is granted by CMP traces, diffuse scattering presents an additional challenge for phase estimation techniques because at a particular time, echoes are received for all points along the isochronous volume, where the time-of-flight to the aperture is identical. In previous works, beamforming is applied in order to increase the SNR at a region of interest while introducing destructive interference at all other locations. However, this does not apply in our case, as we do not introduce a beamforming step and therefore do not know the position of our scattering locations a-priori.

To localize contributions at a defined scattering azimuth direction, we propose to apply delays to account for the a-priori position that we expect a scatterer $\hat{\mathbf{p}}$ at an a-priori sound speed $\hat{c}$. This is akin to a "moveout" operation, and provides approximate time alignment of all time traces of a scattering direction of interest. At this stage, with previous beamforming methods, typically the data would be summed i.e. compounded to increase the SNR. However, instead we apply a linear filter across the time and aperture domains jointly. This spatiotemporal filter provides a passband to allow data in the "neighborhood" of the a-priori sound speed and position $(\hat{\mathbf{p}}, \hat{c})$ to pass, while data that is "far" from the a-priori sound speed and position is rejected. Thereby we filter out scattering contributions off the azimuth direction of interest, while allowing unconstrained capture of signals from a range of speed-of sound values. This is similar to a method explored in [10] where a filter was applied without a-priori time alignment.

## III. Methods

To validate our approach, we generated full synthetic aperture data using 2D simulations of a linear array transducer and diffuse scattering via k-Wave [11]. The simulation parameters are summarized in Table I and the setup is illustrated in 3. The medium had four layers with distinct sound speed values. In order to simulate a pure diffuse scattering media, the average density was adjusted in each layer with respect to the speed of sound to obtain a constant acoustic impedance and avoid specular reflections at layered interfaces. A random density distribution was added to produce diffuse scattering, as in [12]. The ground truth global average sound speed with depth is given by the inverse of the mean slowness from the surface of the transducer up to a given depth.

To evaluate the performance of our sound speed estimation method, we computed the mean error (bias) and the root-mean-square error (RMSE) of the estimated sound speed profile with respect to the ground truth. We exclude near field values for a settling period of 10 microseconds corresponding to an axial depth of about 7 mm. Because we estimate both the sound speed and the depth simultaneously, our RMSE is computed by fitting the estimates to both the ground truth sound speed and ground truth depth jointly.

To verify the robustness of our method to the initial speed-of-sound estimate, we varied the a-priori sound speed from 1450 m/s to 1650 m/s at intervals of 5 m/s. This sound speed choice affects both the a-priori moveout step as well as the spatiotemporal filter.

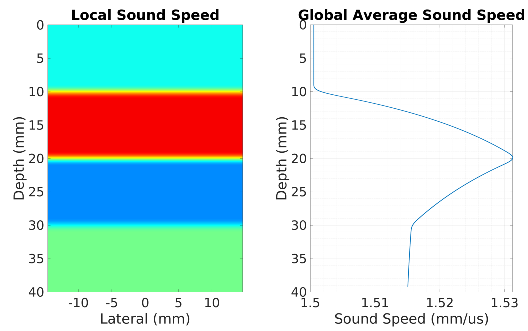


Fig. 3. Sound speed distribution - the four layers in were modelled to be at 1501 m/s, 1565 m/s, 1484 m/s, and 1513 m/s.

TABLE I
k-Wave Simulation Parameters

| Parameter | Value |
|---|---|
| Pitch | 0.150 mm |
| Center Frequency | 8 MHz |
| Fractional Bandwidth | 70% |
| Wavelength | 0.186 - 0.196 mm |
| Grid Spacing | 0.030 mm |
| Sampling Interval | 5.85 ns |

## IV. Results & Discussion

The effect of the spatiotemporal filtering for speed-of-sound estimation at an axial CMP ($0^\circ$) is shown in Fig. 4. Without the filter, due to the clutter from multiple azimuth scattering directions, estimates of the sound speed showed an RMSE of 49.0 m/s and a bias of 41.0 m/s. The errors are larger than the variance in the sound speed itself and therefore no discernable sound-speed trend can be resolved. After application of the filter, the estimator reflects the trend of the data with an RMSE of 1.8 m/s and a bias of 1.3 m/s with a minimum and maximum bias of -4.5 m/s and +8.4 m/s. The sound speed estimates seem to vary between periods of overestimation and underestimation at different depths, probably due to phase estimation noise due to the finite window size of the correlation estimates. The depth estimates however remain consistently spaced and monotonically increasing with depth as we might expect.

Fig. 5 shows the results for speed-of-sound estimates for axial steering and when steering at $10^o$ off axis at different depths. The estimates are originally biased high, but then decrease with depth converging to the nominal phantom speed-of-sound value. Since the described method provides average speed-of-sound estimates with depth, this may be indicative of a larger speed-of-sound value at the phantom surface. Imperfect estimations of the time offset of the transducer and near field effects may lead to similar effects at shallow depths. It should be noted that at a depth of 10 mm (approximately 40 wavelengths), the error is already reduced to less than 10 m/s.

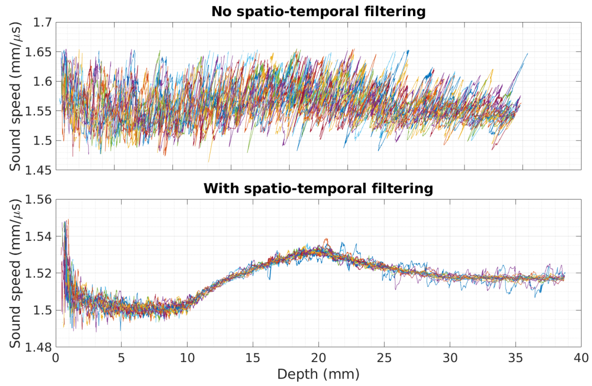


Fig. 4. Estimator performance in simulation: without using the spatio-temporal filter, the results vary greatly and there is no discrenable trend. Using the spatial-temporal filter, the estimator recovers the global average sound speed trend.

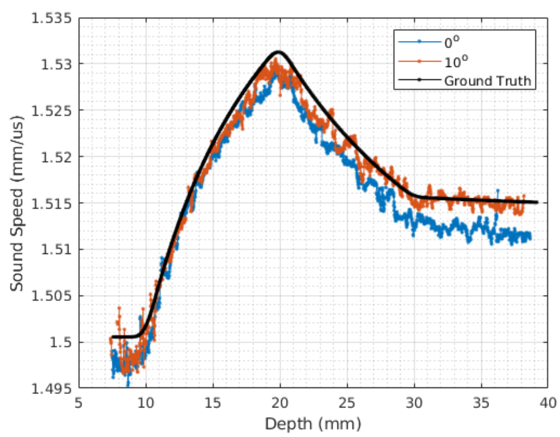


Fig. 5. Axial and non-axial estimation: the estimates of the sound speed when steering at $10^o$ perform as well or better than the estimates at $0^o$.

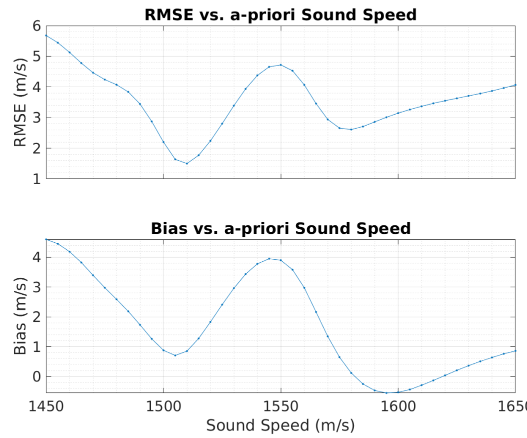


Fig. 6. Estimator RMSE & Bias vs. a-priori sound speed in a simulated 4-layer media model: the method is robust to changes in the a-priori sound speed.

The RMSE and bias of the estimator as we change the a-priori sound speed speed is shown in Fig. 6. The RMSE and bias both reach a local minimum between 1505 m/s and 1510 m/s, which corresponds to the mean global average sound speed of 1515 m/s from between 7.5 mm and 39 mm.

## V. Conclusions and Outlook

In this work we have introduced a novel method for global average sound speed estimation from full synthetic aperture data which avoids the fundamental spatial ambiguity problem that occurs when beamforming and creating an image. We validated our approach in simulation and demonstrated it's robustness to the a-priori knowledge of the sound speed in the medium. This work lays a basis for using tomographic approaches to reconstruct the local sound speed as well as using the global average sound speed for aberration correction.

## References

[1] Arsenii V Telichko, Rehman Ali, Thurston Brevett, Huaijun Wang, Jose G Vilches-Moure, Sukumar U Kumar, Ramasamy Paulmurugan, and Jeremy J Dahl. Noninvasive estimation of local speed of sound by pulse-echo ultrasound in a rat model of nonalcoholic fatty liver. *Physics in Medicine & Biology*, 67(1):015007, January 2022.

[2] Marion Imbault, Alex Faccinetto, Bruno-Félix Osmanski, Antoine Tissier, Thomas Deffieux, Jean-Luc Gennisson, Valérie Vilgrain, and Mickaël Tanter. Robust sound speed estimation for ultrasound-based hepatic steatosis assessment. *Physics in Medicine and Biology*, 62(9):3582–3598, apr 2017.

[3] L. Ruby, S. J. Sanabria, N. Saltybaeva, T. Frauenfelder, H. Alkadhi, and M. B. Rominger. Comparison of ultrasound speed-of-sound of the lower extremity and lumbar muscle assessed with computed tomography for muscle loss assessment. *Medicine (Baltimore)*, 100(21):e25947, May 2021.

[4] Nebojsa Duric, Peter Littrup, Priti Chandiwala-Mody, Cuiping Li, Steven Schmidt, Lukasz Myc, Olsi Rama, Lisa Bey-Knight, Jessica Lupinacci, Bryan Ranger, Amy Szczepanski, and Erik West. In-vivo imaging results with ultrasound tomography: report on an ongoing study at the karmanos cancer institute. In Jan D'hooge and Stephen A. McAleavey, editors, *SPIE Proceedings*. SPIE, March 2010.

[5] Lisa Ruby, Sergio J. Sanabria, Katharina Martini, Konstantin J. Dedes, Denise Vorburger, Ece Oezkan, Thomas Frauenfelder, Orcun Goksel, and Marga B. Rominger. Breast cancer assessment with pulse-echo speed of sound ultrasound from intrinsic tissue reflections. *Investigative Radiology*, 54(7):419–427, July 2019.

[6] Peter R Hoskins, Kevin Martin, and Abigail Thrush, editors. *Diagnostic Ultrasound*. CRC Press, April 2019.

[7] Patrick Stähli, Maju Kuriakose, Martin Frenz, and Michael Jaeger. Improved forward model for quantitative pulse-echo speed-of-sound imaging. *Ultrasonics*, 108:106168, 2020.

[8] Sergio J Sanabria, Ece Ozkan, Marga Rominger, and Orcun Goksel. Spatial domain reconstruction for imaging speed-of-sound with pulse-echo ultrasound: simulation and iin vivo/i study. *Physics in Medicine & Biology*, 63(21):215015, oct 2018.

[9] Rehman Ali, Thurston Brevett, Dongwoon Hyun, Leandra L. Brickson, and Jeremy J. Dahl. Distributed aberration correction techniques based on tomographic sound speed estimates. *IEEE Transactions on Ultrasonics, Ferroelectrics, and Frequency Control*, 69(5):1714–1726, 2022.

[10] M.A. Haun, D.L. Jones, and W.D. Oz. Overdetermined least-squares aberration estimates using common-midpoint signals. *IEEE Transactions on Medical Imaging*, 23(10):1205–1220, 2004.

[11] B. E. Treeby and B. T. Cox. k-Wave: MATLAB toolbox for the simulation and reconstruction of photoacoustic wave fields. *J Biomed Opt*, 15(2):021314, 2010.

[12] Gianmarco F. Pinton, Gregg E. Trahey, and Jeremy J. Dahl. Spatial coherence in human tissue: implications for imaging and measurement. *IEEE Transactions on Ultrasonics, Ferroelectrics, and Frequency Control*, 61(12):1976–1987, 2014.